Journal of Anatomy

J. Anat. (2009) **214**, pp926–936 doi: 10.1111/j.1469-7580.2009.01084.x

Three-dimensional morphometric analysis of brain shape in nonsyndromic orofacial clefting

Seth M. Weinberg, Nancy C. Andreasen and Peg Nopoulos

Psychiatry Iowa Neuroimaging Consortium, Department of Psychiatry, University of Iowa Hospital and Clinics, Iowa City, IA, USA

Abstract

Previous studies report structural brain differences in individuals with nonsyndromic orofacial clefts (NSOFC) compared with healthy controls. These changes involve non-uniform shifts in tissue volume within the cerebral cortex and cerebellum, suggesting that the shape of the brain may be altered in cleft-affected individuals. To test this hypothesis, a landmark-based morphometric approach was utilized to quantify and compare brain shape in a sample of 31 adult males with cleft lip with or without cleft palate (CL/P), 14 adult males with cleft palate only (CPO) and 41 matched healthy controls. Fifteen midline and surface landmarks were collected from MRI brain scans and the resulting 3D coordinates were subjected to statistical shape analysis. First, a geometric morphometric analysis was performed in three steps: Procrustes superimposition of raw landmark coordinates, omnibus testing for group difference in shape, followed by canonical variates analysis (CVA) of shape coordinates. Secondly, Euclidean distance matrix analysis (EDMA) was carried out on scaled inter-landmark distances to identify localized shape differences throughout the brain. The geometric morphometric analysis revealed significant differences in brain shape among all three groups ($P < 0.001$). From CVA, the major brain shape changes associated with clefting included selective enlargement of the anterior cerebrum coupled with a relative reduction in posterior and/or inferior cerebral portions, changes in the medio-lateral position of the cerebral poles, posterior displacement of the corpus callosum, and reorientation of the cerebellum. EDMA revealed largely similar brain shape changes. Thus, compared with controls, major brain shape differences were present in adult males with CL/P and CPO. These results both confirm and expand previous findings from traditional volumetric studies of the brain in clefting and provide further evidence that the neuroanatomical phenotype in individuals with NSOFC is a primary manifestation of the defect and not a secondarily acquired characteristic.

Key words: brain; clefting; Euclidean distance matrix analysis; geometric morphometrics; magnetic resonance imaging; shape.

Introduction

Structural brain abnormalities are often present in individuals with major craniofacial malformations (Bergsma, 1975; Sulik & Johnston, 1982; Vermeij-Keers et al. 1983). This co-occurrence reflects the intimate developmental relationship between the face and the brain (Kjaer, 1995; Schneider et al. 2001; Marcucio et al. 2005). At the cellular level, the mesenchymal tissue making up the paired structures that will eventually coalesce to form the embryonic face is originally derived from neural crest cells situated along the dorsal margins of the primordial brain (Le Douarin & Kalcheim, 1999; Graham, 2003). Consequently, defects in neural crest cell identity or migration patterns are a major source of craniofacial anomalies, including some orofacial clefts (Jones, 2006). Developmental brain–face interactions also occur at the gross structural level. By the fourth week of development, the frontonasal prominence, situated immediately adjacent to the rapidly expanding forebrain, dominates the nascent face (Hinrichsen, 1985). Derivatives of the frontonasal prominence include the nasal prominences that form the structural basis for the primary palate (Sperber, 2001; Senders et al. 2003). The proper spatial positioning of the nasal prominences relative to one another and to the maxillary prominences is a critical factor in facilitating normal palatogenesis and depends in part on the growth trajectory of the forebrain (Diewert et al. 1993; Jiang et al. 2006). Altered early brain development, therefore, may be an important risk factor for orofacial clefting and is likely to manifest in altered patterns of brain morphology. Multiple lines of evidence suggest that orofacial clefting is associated with a distinctive neuroanatomical phenotype. For instance, differences in frontonasal prominence morphology have been reported in the embryos of mice with

Correspondence
Seth M. Weinberg, 200 Hawkins Drive, W278 GH, Iowa City, IA 52242, USA. T: + 1 319 3538536; F: + 1 319 3845532; E: seth-m-weinberg@uiowa.edu

Accepted for publication *15 March 2009*

high rates of spontaneous clefting compared to non-susceptible strains (Young et al. 2007; Parsons et al. 2008). Similarly, adult mice predisposed to clefting were found to display changes in calvarial shape, although this is a crude index of brain shape (Hallgrímsson et al. 2004).

Most of our knowledge about the brain phenotype in orofacial clefting comes from comparative morphological studies in humans. Extensive morphological differences have been reported in the brains of individuals affected with nonsyndromic orofacial clefts (NSOFC) compared with healthy controls. Using MR imaging technology to quantitatively assess the structure of the brain, Nopoulos and coworkers (2002) reported that adult males with NSOFC had selective enlargement of anterior-superior portions of the cerebrum (frontal and parietal lobes) coupled with volume reductions in posterior-inferior cerebral regions (occipital and temporal lobes) and the cerebellum compared with matched controls. These regional differences were often tissue-specific in nature; e.g. differences in frontal lobe, parietal lobe and cerebellar volume were driven principally by shifts in gray matter. A somewhat distinct, yet equally compelling, constellation of brain changes was recently reported in an adolescent NSOFC sample (Nopoulos et al. 2007a). In addition, individuals with NSOFC have been shown to possess a higher than normal rate of midline developmental brain anomalies, such as pathologically enlarged cavum septi pellucidi (Nopoulos et al. 2001) and corpus callosum atrophy (Mueller et al. 2007; Calzolari et al. 2007). In general, the degree of alteration in brain morphology has been found to correlate in a predictable manner with reduced cognitive performance (Nopoulos et al. 2001, 2002; Shriver et al. 2006). Indirect markers for brain lateralization, such as handedness, have also been shown to differ in NSOFC populations (Fraser & Rex, 1985; Yorita & Melnick, 1988; Wentzlaff et al. 1997; Jeffery & Boorman, 2000). These findings suggest that the brain itself is fundamentally different in individuals with NSOFC and provide persuasive evidence that the various cognitive deficits associated with the anomaly (Richman, 1980; Broen et al. 1998) are in fact manifestations of a primary brain abnormally.

The non-uniform nature of the shifts in tissue volume within the cerebral cortex and cerebellum suggest that the overall shape of the brain may be altered in cleft-affected individuals. Changes in brain shape may reflect disturbances in early brain morphogenesis and may be an important factor in NSOFC liability due to the influence of brain geometry on the developing craniofacial complex. Quantitative analysis of the brain phenotype in humans with NSOFC has been limited thus far to the conventional volumetric approach, which can only provide limited and indirect information about brain shape. Because of its complex three-dimensional structure, assessing the shape of the brain requires morphometric methods capable of incorporating and preserving the brain's intrinsic geometry. In the present study, we employ two different methods of shape analysis based on 3D landmark coordinate data to test the hypothesis that individuals with NSOFC possess a distinctive brain shape. An important aspect of this approach is that it simultaneously incorporates information on both surface anatomy and midline structures, allowing for a morphometric assessment of brain regions largely ignored in previous studies. As a result, this study may offer some novel insights into the developmental processes underlying the neuroanatomical phenotype in orofacial clefting.

Materials and methods

Subjects

Following approval from our local ethics committee, study subjects were initially identified through the University of Iowa Cleft Lip and Palate Registry, a large database comprising cleft patients treated at the University of Iowa's Craniofacial Center. Following an exhaustive medical chart review, 46 adult males with NSOFC were recruited. One subject was subsequently dropped from the analysis due a problem with his MR scan. Of the remaining 45 subjects, 31 had cleft lip with or without cleft palate (CL/P; 11 bilateral, 17 left unilateral, 3 right unilateral), and 14 had cleft palate only (CPO), which is considered an etiologically distinct condition on developmental and epidemiological grounds. The case sample was limited to adult males (> 18 years of age) to mitigate potential gender and age differences on brain morphology (Nopoulos et al. 2000; Goldstein et al. 2001; Sowell et al. 2007).

Healthy adult males (n = 41) were identified through an existing pool of normal controls that had previously participated in brain imaging research conducted as part of the Schizophrenia Research Program at the University of Iowa. Cases and controls were of Caucasian ancestry, reflecting the population of Iowa. Informed consent was obtained for all subjects prior to participation. The mean age of the control sample was 28.8 (7.5) years, compared to 30.1 (7.1) years for the NSCLP sample. This difference was not statistically significant ($P > 0.05$).

Image acquisition and landmarking

MR images of the brain were obtained using a 1.5 Tesla GE Signa scanner. Multispectral MR data were acquired with the implementation of three different imaging sequences. Three-dimensional T1-weighted images were acquired using a SPGR sequence with the following parameters: TE = 5 ms; TR = 24 ms; flip angle = 40; NEX = 2; FOV = 26 cm; matrix = 256 × 192; slice thickness = 1.5 mm. Two-dimensional proton density (PD) and T2-weighted images were obtained using the following sequence: TE = 96 ms (36 ms for PD); TR = 3000 ms; NEX = 1; FOV = 26 cm; matrix = 256 × 192; echo train length = 1. The same imaging sequence parameters were used on cases and controls, and all scans were screened for overall quality and motion artifacts. Image processing was carried out using the BRAINS software package (Andreasen et al. 1992; Magnotta et al. 1999a, 2002). MR images were aligned along the three principle axes and resampled to 1.0 mm^3 voxels. Automated methods were used to generate 3D models of the cortical surface from the individual brain slices (Magnotta et al. 1999b).

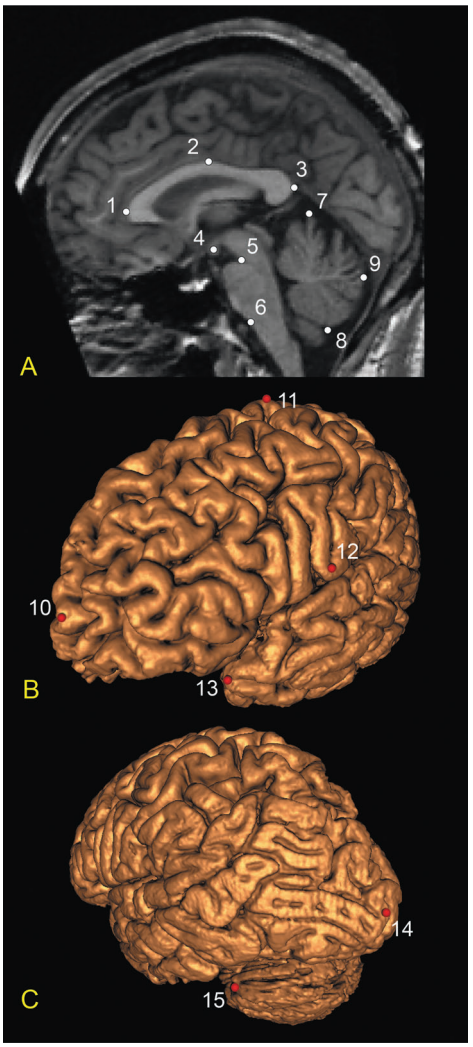

Fig. 1 Brain landmarks used in the present study: (A) T1-weighted mid-sagittal slice showing midline landmarks; (B) frontolateral view of the 3D reconstructed left cerebral surface with landmarks; (C) posterolateral view of the 3D reconstructed left cerebral and cerebellar surface with landmarks. Midline landmarks: 1, anterior corpus callosum; 2, superior corpus callosum; 3, posterior corpus callosum; 4, centroid of mammillary body; 5, superior pons; 6, inferior pons; 7, superior cerebellum; 8, inferior cerebellum; 9, posterior cerebellum. Surface landmarks: 10, left frontal pole; 11, left vertex (on precentral gyrus); 12, left occipital pole; 13, left temporal pole; 14, left inferior termination of central sulcus; 15, left maximum cerebellar breadth.

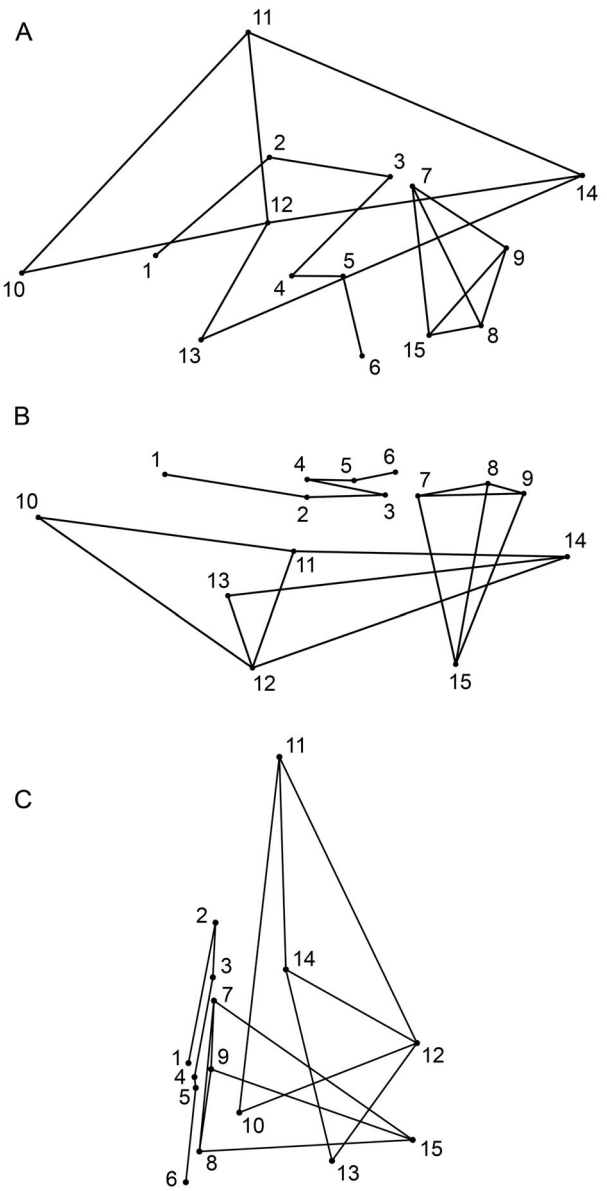

Fig. 2 Wireframe models of the brain constructed from the 15 midline and left cerebral surface landmarks: (A) lateral view; (B) superior view; (C) anterior view. Landmarks are numbered as in Fig. 1.

Using the landmarking module within the BRAINS package, 15 landmarks were digitized on each subject's T1-weighted image (Figs 1 & 2). Nine midline landmarks were selected from the image corresponding to the mid-sagittal plane. For the six remaining brain surface landmarks, points were selected on one of the three orthogonal planes (coronal, axial or sagittal) and their locations verified on the 3D-generated surface. All six surface landmarks were collected on the left side only. Landmarks were chosen on the basis of reliability, maximizing anatomical coverage, and prior morphological descriptions of the brain in orofacial clefting. All landmarks were collected by a single observer (S.M.W.) blind to affection status. Following selection, the XYZ coordinates for each subject's complete landmark set were saved for later analysis.

Intra-observer error associated with landmark localization was assessed by digitizing the full set of landmarks twice on an independent sample of 20 individuals. At least 1 week was allowed to elapse between the first and second landmarking session to minimize recall bias. Intra-class correlation coefficients (ICC) were computed for each landmark in each of the three principal axes. An ICC of 0.80 was considered the threshold for acceptable error. All 15 landmarks demonstrated high precision (X-axis ICC range: 0.98–1.00; Y-axis ICC range: 0.86–1.00; Z-axis ICC range: 0.88–1.00) and were retained for analysis.

Statistical approach

Two different approaches were utilized to compare brain shape across CL/P cases, CPO cases, and healthy controls: geometric morphometrics and Euclidean distance matrix analysis (EDMA). For the geometric morphometric analysis, 3D landmark coordinates for each subject were aligned using Procrustes superimposition. The purpose of this procedure is to fit the data into a common coordinate system through an iterative least-squares routine to center, scale, and rotate the individual landmark configurations (Rohlf & Slice, 1990). The result is a new set of 3D coordinates (Procrustes coordinates) that preserves information on shape. The Procrustes coordinates were then subjected to an omnibus shape test (Goodall's F-test), which evaluates the null hypothesis that mean shape is equivalent across groups (Goodall, 1991). Both standard and permutation versions of the F-test for shape difference were carried out using the IMP program Simple3D (Sheets, 2004).

To carry out traditional parametric statistics on shape coordinate data, the Procrustes coordinates were projected from non-Euclidean shape space to a linear tangent space (Rohlf, 1999). Canonical variates analysis (CVA) was then applied to the tangent-projected Procrustes coordinate data (Zelditch et al., 2004) to test for and describe group differences in brain shape. CVA is a multivariate data reduction method, computationally similar to discriminant function analysis, where the variance parameters are optimized to maximally discriminate among groups. Each canonical variate (CV) is a linear combination of variables (i.e. shape coordinates), weighted to reflect a distinct mode of shape variation. In the context of shape analysis, the ultimate goal of CVA is to uncover aspects of shape variation that best distinguish among existing groups in a dataset. Because the geometric morphometric approach preserves the intrinsic geometry of landmark coordinate data, shape variation along a given CV can be visualized as a displacement of points in 3D space, providing an intuitive approach to visualize group differences in shape (O'Higgins & Jones, 1998). CVA was performed in MorphoJ v1.0 (Klingenberg, 2008).

EDMA represents an alternative approach to the comparison of form/shape across groups based on inter-landmark distances (Lele & Richtsmeier, 2001; Richtsmeier et al. 2002). In EDMA, the form of an object is defined by the complete set (or matrix) of linear distances between all possible landmark pairs; thus, for a form comprising 15 landmarks, there will be 15(15 – 1)/2, or 105, linear distances. The analysis of shape is accomplished by scaling each subject's complete set of linear distances prior to analysis by some measure of size (e.g. the geometric mean). The mean shape matrix for a group is determined by averaging across each member's matrix of scaled inter-landmark distances. The statistical comparison of shape is based on the arithmetic differences between the mean shape matrices of two groups and is performed in both an omnibus and an element-wise fashion. In the omnibus test, the goal is to determine whether two mean shapes are equivalent overall. In element-wise testing, the goal is to facilitate the discovery of morphological regions where shape differences are most conspicuous between groups. For both types of tests, statistical significance is determined by empirical confidence intervals generated via random bootstrap re-sampling routines. When a given confidence interval contains zero (indicating no difference), this is regarded as evidence of equivalence across groups. For the present study, 95% confidence intervals were used for all tests. All analyses were performed using the SHAPE module within the EDMA statistical package for Windows, WinEDMA v1.0.1 (Cole, 2003). All other statistical tests were performed in SPSS v15 (Chicago, IL).

Table 1 Between-group distance statistics: Procrustes distances above the diagonal and Mahalanobis distances below the diagonal

	CL/P	CPO	Controls
CL/P	–	0.032*	0.028*
CPO	3.127*	–	0.029*
Controls	2.923*	2.983*	–

*$P < 0.001$ based on permutation testing.

Because EDMA is based on a definition of form that is invariant to the nuisance parameters of translation, rotation and reflection, it obviates the need to fit landmark data into a common coordinate system prior to the comparison of shape. This is the most striking difference between EDMA and Procrustes-based approaches. There is a long-standing debate regarding the merits (and limitations) of these alternative morphometric methods. Addressing these concerns is beyond the score of this paper; interested readers should see Rohlf (2000) and Richtsmeier et al. (2002) for a detailed discussion. Both methods have been used to investigate biological shape in a wide variety of human and non-human populations. In accordance with a growing community of researchers (e.g. Hallgrímsson et al. 2004), we take the pragmatic view that these approaches are largely complementary and that their combined use can provide a more complete picture than either method in isolation.

Results

Omnibus shape testing

A series of Goodall's *F*-tests was performed on the Procrustes aligned coordinates to compare brain shape across the three study groups. As shown in Table 1, all three groups demonstrated significant shape differences from one another based on permutation testing (400 iterations): CL/P vs. controls (Procrustes distance = 0.028; $F = 2.065$; $P < 0.001$), CPO vs. controls (Procrustes distance = 0.029; $F = 1.374$; $P < 0.001$), CL/P vs. CPO (Procrustes distance = 0.032; $F = 1.674$; $P < 0.001$). The level of within-group variance in shape, however, was equivalent across groups based on permutation testing: CL/P vs. controls (delta $V = 0.00075$; $P > 0.05$), CPO vs. controls (delta $V = 0.00192$; $P > 0.05$), CL/P vs. CPO (delta $V = 0.00117$; $P > 0.05$).

Canonical variates analysis

CVA of tangent space Procrustes coordinates resulted in the extraction of two canonical variates describing 100% of the shape variation in the dataset. These two CVs produced significant group separation as evidenced by the Mahalanobis distance statistics shown in Table 1 and by the pattern of group clustering depicted in Fig. 3. CV1 accounted for 64.4% of the shape variance and was associated principally with separation of CL/P cases from controls, with CPO cases intermediate between these two groups. The specific brain shape changes associated with

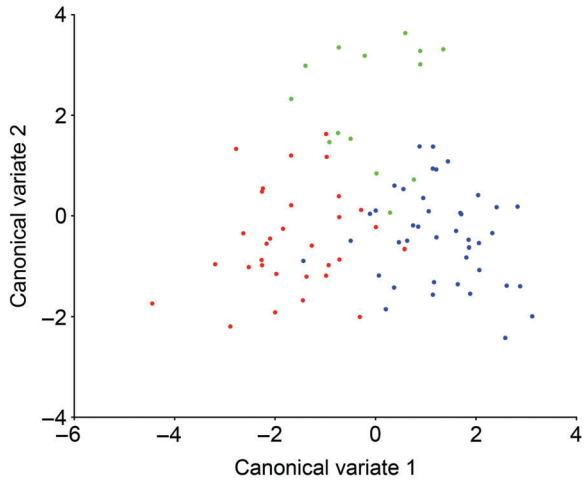

Fig. 3 Plot of scores on CV1 and CV2 for all 86 subjects based on their Procrustes coordinate data. Groups are color-coded: CL/P = Red; CPO = Green; Controls = Blue.

CV1 are depicted in Fig. 4 as wireframe deformations. Compared with controls, the CL/P group was characterized by a tissue distribution shift in the cerebrum, such that the anterior cerebrum (i.e. frontal lobe) was enlarged relative to the posterior and inferior cerebrum (i.e. occipital and temporal lobes). This shift was mainly due to the inferior-anterior displacement of the frontal pole (landmark 10), superior-posterior displacement of vertex (landmark 11), superior-posterior displacement of the temporal pole (landmark 13), and anterior displacement of the occipital pole (landmark 14). The entire cerebrum in the CL/P group also showed evidence of narrowing along the medio-lateral axis, which is most apparent in Fig. 4C. Concomitant changes included posterior displacement of the corpus callosum (landmark 2), lateral displacement of the frontal and occipital poles (landmarks 10 and 14) away from the midline, and shifts in cerebellar orientation and shape (increased forward tilt, reduction in vertical height and lateral expansion/elongation).

CV2 accounted for the remaining 35.6% of the shape variance and was associated principally with the separation of CPO individuals from the other groups (Fig. 3). As indicated in Fig. 5, the shape changes that characterize the CPO group include vertical shortening and general elongation of the cerebrum. As in CL/P, the tissue distribution is altered in the CPO cerebrum such that the frontal lobe occupies a relative larger portion of the brain while the more posterior and inferior lobes are proportionally reduced. This shift, however, is achieved through a slightly different set of landmark displacements, e.g. inferior-anterior shift of vertex (landmark 11) and posterior shift of the central sulcus termination point (landmark 12). Furthermore, the anterior and posterior poles of the cerebral cortex are displaced medially, given the brain a more convex appearance (Fig. 5C). Additional shape changes include a slight inferior and posterior displacement of the entire corpus callosum, a more vertical orientation of the brain stem (landmarks 5 and 6), and a reorientation of the cerebellum involving superior displacement of the midline points (landmarks 7, 8 and 9) and elongation due to the concomitant inferior-anterior-lateral displacement of landmark 15 (maximum cerebellar breadth).

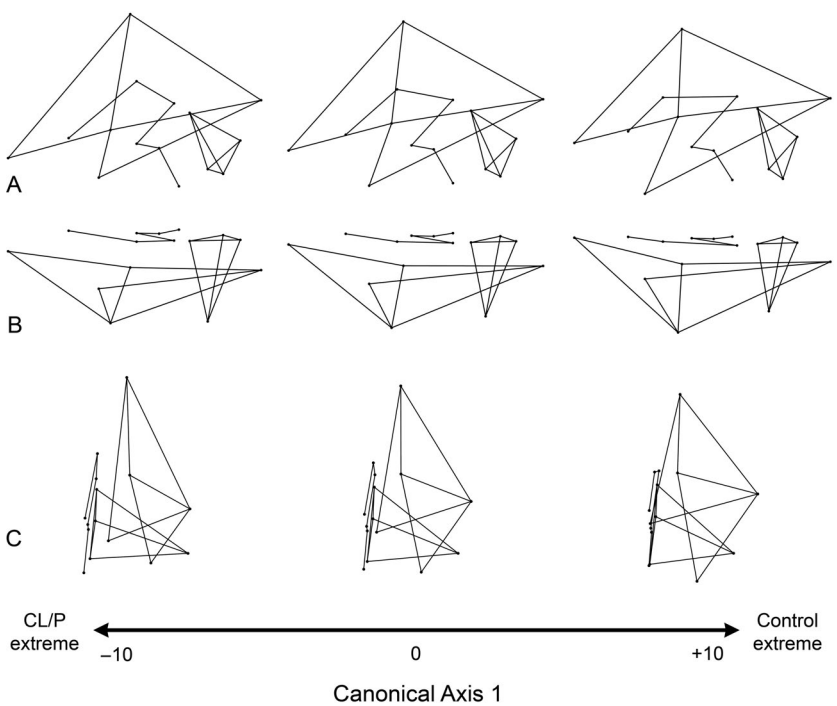

Fig. 4 Brain shape variation associated with CV1, separating CL/P cases from healthy controls. The wireframe models represent the nature of the shape change along the first canonical discrimination axis. The middle wireframe represents the shape of the brain when the score on CV1 is zero. The wireframes at the negative end of the canonical axis show brain shape changes associated with CL/P. Three principle views are provided: (A) lateral; (B) superior; (C) anterior. See Figs 1 and 2 for landmark definitions.

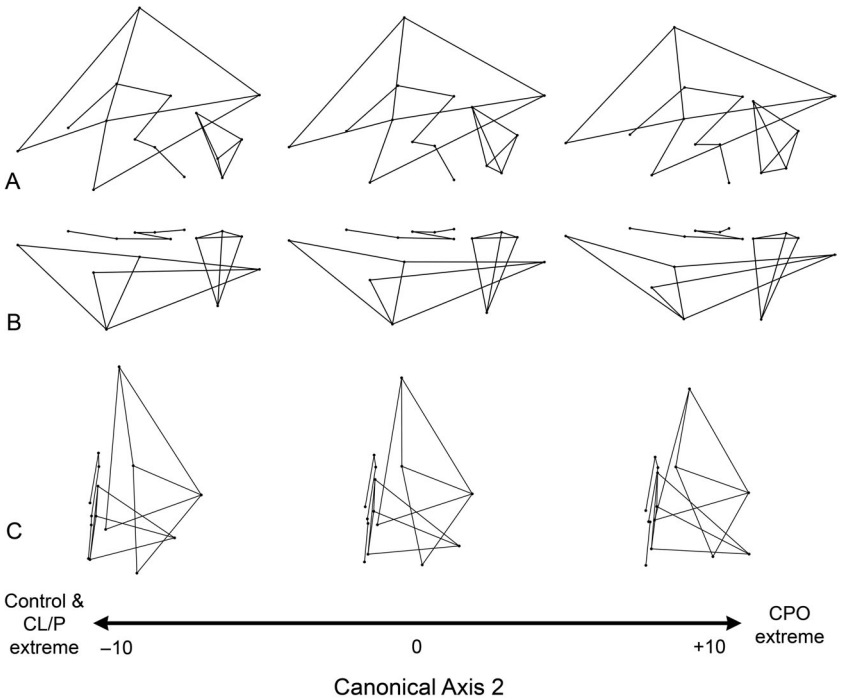

Fig. 5 Brain shape variation associated with CV2, separating CPO cases from the remaining groups. The wireframe models represent the nature of the shape change along the second canonical discrimination axis. The middle wireframe represents the shape of the brain when the score on CV2 is zero. The wireframes at the positive end of the canonical axis show brain shape changes associated with CPO. Three principle views are provided: (A) lateral; (B) superior; (C) anterior. See Figs 1 and 2 for landmark definitions.

Euclidean distance matrix analysis

EDMA demonstrated both omnibus and element-wise differences in brain shape among all three groups ($P < 0.05$). Element-wise testing revealed that the major shape differences were localized to a number of distinct brain regions, including portions of the cerebrum, cerebellum, corpus callosum and brain stem. Figure 6 shows the individual shape variables (scaled linear distances) that differ with the greatest magnitude between groups. These variables coconstitute the upper and lower 10% of the distribution of 105 shape difference scores when sorted by magnitude. Compared with controls, the CL/P group was characterized by a combination of frontal lobe enlargement, temporal lobe reduction, and posterior displacement of the corpus callosum. The CPO group displayed evidence of temporal lobe reduction, anterior-posterior cerebral lengthening, lateral elongation of the cerebellum and a posterior shift in the position of the termination of the central sulcus (landmark 12) relative to the healthy control group. When the two case groups were compared to each other directly, the CPO brain showed reduced cerebral height, increased cerebral length, posterior displacement of the central sulcus termination and a more vertical orientation of the brain stem.

Discussion

Prior volumetric studies of the brain in individuals with NSOFC report region- and tissue-specific patterns of structural disturbance. In a previous study comparing brain structure in affected adult males and healthy matched controls, no changes in overall brain or cerebral size were observed (Nopoulos et al. 2002). However, when individual brain regions were considered, a number of significant differences emerged. Adult males with NSOFC demonstrated significant enlargement of the frontal and parietal lobes coupled with significant reduction of the temporal and occipital lobes and cerebellum. The non-uniform and highly regionalized nature of the observed brain volume changes in this sample suggests that the entire shape profile of the brain is altered in orofacial clefting. This was confirmed in the present study, as affected cases demonstrated a significant shift in overall brain shape. Moreover, the pattern of regional shape change in the cerebrum was consistent with previous volumetric findings; adult males with NSOFC (both CL/P and CPO) displayed evidence of selective enlargement of the anterior cerebrum coupled with relative reductions in more posterior and inferior cerebral portions. There was also evidence in the CL/P group of lateral displacement of the frontal and occipital poles, posterior displacement of the corpus callosum, and reorientation of the cerebellum (relative increase in breadth). The CPO group displayed many similar brain changes (relative to controls); however, this group also demonstrated a unique tendency toward an overall longer and vertically shorter cerebrum along with medial displacement of the frontal and occipital poles. These shape differences may ultimately reflect the etiologically distinct nature of the two conditions (Jugessur & Murray, 2005). Taken together, these findings indicate that orofacial clefting is associated with prominent shape differences involving multiple brain regions and tissues.

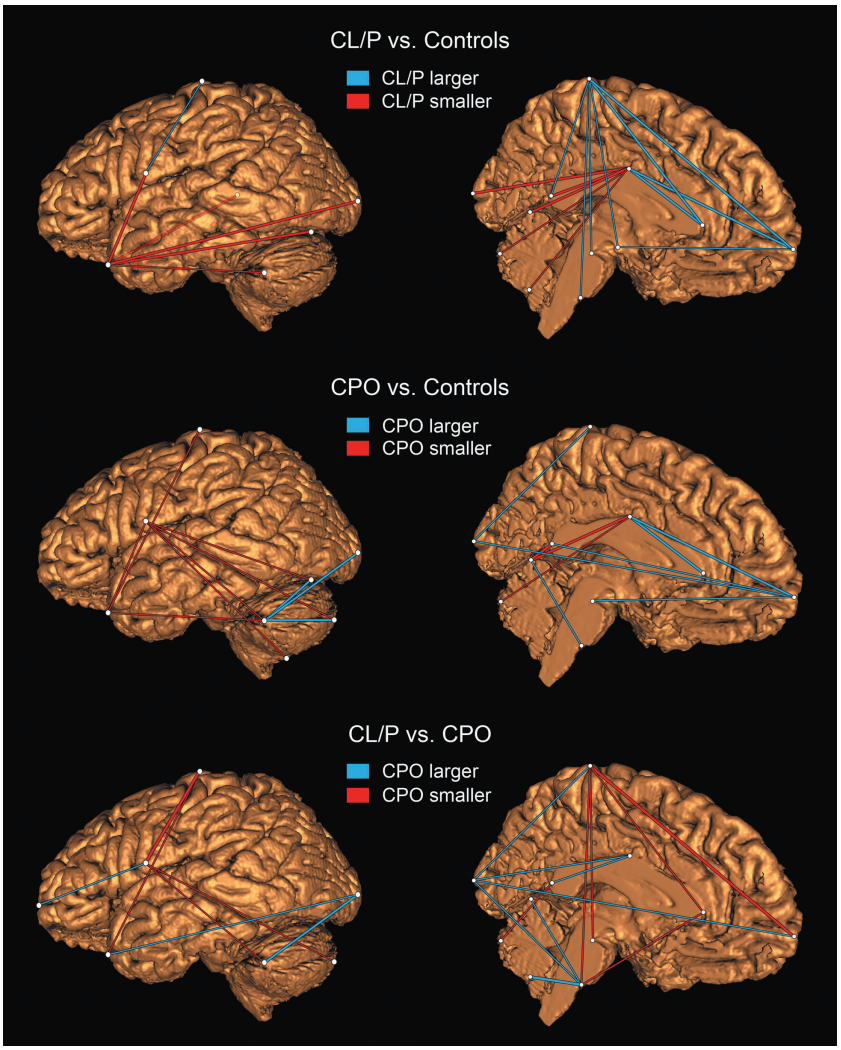

Fig. 6 Shape variables (scaled linear distances) showing the greatest degree of difference between groups from EDMA. As explained in the figure, the color of the lines shows the direction of change. The variables shown here represent the upper and lower 10% of the sorted shape difference matrix; i.e. distances with the greatest group difference in either direction. Variables where this difference was statistically significant ($P < 0.05$) are represented by thicker lines. For each group comparison two views are included: a sagittal view of the left cerebral and cerebellar outer surface, and an internal mid-sagittal view of the left brain hemisphere. Note: the line connecting the temporal pole to the posterior corpus callosum in the first row (CL/P vs. Controls) is rendered semi-transparent to facilitate visualization.

The observed increase in the anterior cerebrum relative to the posterior and inferior cerebrum is the result of a major tissue distribution shift in the NSOFC brain. A similar anterior-posterior pattern of tissue allocation has been described in other genetic syndromes that feature clefting as part of their phenotype, including velocardiofacial syndrome (Eliez et al. 2000; Kates et al. 2001; Campbell et al. 2006) and Van der Woude syndrome (Nopoulos et al. 2007b). Furthermore, reductions in the posterior neurocranium were recently reported in CL/P-susceptible mice (Hallgrímsson et al. 2004; Parsons et al. 2008), suggesting a similar shape profile for the underlying brain. The mechanisms responsible for this change in brain shape are unclear, but likely reflect processes at work during early brain development. Experiments on avian and mouse embryos have documented an intricate molecular dialogue involving signals emanating from the forebrain and the overlying frontonasal tissues that give rise to much of the upper and middle face (Francis-West et al. 2003; Hu et al. 2003; Creuzet et al. 2004; Marcucio et al. 2005; Bertrand & Dahmane, 2006; Halilagic et al. 2007). This signaling network includes growth factors and morphogens such as *FGF8* and *SHH*, which play an important role in both brain morphogenesis and facial prominence outgrowth (Schneider et al. 2001; Jeong et al. 2004; Abzhanov et al. 2007) and are considered gene candidates for CL/P (Orioli et al. 2002; MacDonald et al. 2004; Jiang et al. 2006; Rice et al. 2006; Sasaki et al. 2007; Thomason et al. 2008). *SHH* expression levels, in particular, appear to be related to the growth trajectory of the entire frontonasal mass (Hu & Helms, 1999). Localized overexpression of *SHH* may explain the differential increase in frontal lobe proportions in individuals with orofacial clefts as well as other related phenotypes such as mild hypertelorism, which is present to some degree in both affected cases and their biological relatives (Aduss et al. 1974; Weinberg et al. 2006b).

In the present study, both cleft groups displayed shape changes in the corpus callosum, although these changes were more pronounced in the CL/P subset. Specifically, there was a posterior displacement of the point of maximal

midbody curvature, resulting in a shift of the entire shape profile of the corpus callosum. Morphological changes in the corpus callosum are typically related to disturbances in early brain development (Bookstein et al. 2001; Richards et al. 2004). Changes in corpus callosum size and shape have been documented in a number of disorders with a developmental basis including schizophrenia (Downhill et al. 2000; Narr et al. 2000), fetal alcohol syndrome (Bookstein et al. 2001), Williams syndrome (Tomaiuolo et al. 2002), velocardiofacial syndrome (Shashi et al. 2004; Antshel et al. 2005; Machado et al. 2007) and autism (Boger-Megiddo et al. 2006; Kilian et al. 2008). Although this is the first study to document changes in the shape of the corpus callosum in NSOFC, others have reported midline brain abnormalities in affected individuals. In a recent European cohort study, Mueller et al. (2007) found a 13-fold increase in central nervous system malformations in CL/P cases without a known syndrome compared to the general population; the most common malformation was corpus callosum agenesis. Furthermore, orofacial clefting is associated with an increased frequency of pathologically enlarged cavum septi pellucidi (Nopoulos et al. 2001), which results when the midline cavity that forms between the lateral ventricles fails to fuse in the fetal brain (Sarwar, 1989; Bodensteiner & Schaefer, 1990). These findings suggest that a major disturbance in the formation of midline structures characterizes the NSOFC brain. It is unclear, however, what processes are driving this pattern of dysmorphology. Are the changes intrinsic or secondary to a set of broader morphological shifts occurring within the brain? It is clear that the development of midline brain structures is intimately related to the surrounding anatomy (Richards et al. 2004). Shape differences in the corpus callosum, for instance, have been linked to changes in ventricular size and shape (Casanova et al. 1990; Downhill et al. 2000; Simon et al. 2005; Machado et al. 2007). The results of our CVA of brain shape revealed that proportional shifts in the cerebrum appear to be linked to shape changes in the corpus callosum; in other words, these structures displayed an integrated pattern of shape variation. This suggests that the midline morphological disturbances observed in orofacial clefting either result from or share a common origin with broader changes in cerebral structure.

The finding of altered brain structure in nonsyndromic orofacial clefting has added a new wrinkle to the debate over the factors that shape the cognitive, behavioral and speech/language deficits so often seen in those affected with orofacial clefts (Brennan & Cullinan, 1974; Fox et al. 1978; Kommers & Sullivan, 1979; Richman, 1980; Richman & Elaison, 1993; Neiman & Savage, 1997; Broen et al. 1998). The traditional view has been that these deficits are secondary manifestations of the hearing and/or speech problems typical in affected individuals (Estes & Morris, 1970; Sak & Ruben, 1982). The results of the current study as well as previous studies on brain structure in orofacial clefting challenge this perspective. Our findings suggest that these deficits stem from a primary brain abnormality, the result of a fundamentally altered pattern of brain development. This perspective is supported by the numerous similarities between the kinds of changes in brain shape reported here in orofacial clefting and those observed in other congential developmental conditions. Moreover, previous studies from our laboratory have found direct relationships between abnormalities in brain structure and the psychological sequelae associated with clefting: cognitive deficits (Nopoulos et al. 2002; Shriver et al. 2006), behavioral dysfunction (Nopoulos et al. 2005; Boes et al. 2007) and speech difficulties (Conrad et al. personal communication).

The presence of primary brain abnormalities may have important implications for the clinical management of NSOFC cases. Moreover, including brain abnormalities as part of the phenotypic spectrum of clefting has the potential to improve efforts designed to detect the underlying causes of NSOFC. In recent years, renewed attention has been paid to documenting the full range of phenotypic features associated with clefts of the primary and/or secondary palate, with particular emphasis on subclinical manifestations in non-cleft family members (Weinberg et al. 2006a, 2008; Marazita, 2007). Detailed phenotypic assessments, including an evaluation of brain morphology, in both affected individuals and their unaffected relatives are necessary for understanding how different cleft-related phenotypes are distributed both within and between families. Whether structural brain changes are ubiquitous or present in only a subset of affected cases/families is of pressing concern. As clefting is an etiologically heterogeneous trait, involving disruptions in any of a number of genetic pathways (Stanier & Moore, 2004; Jugessur & Murray, 2005; Lidral & Moreno, 2005), methods capable of linking particular genetic causes to specific phenotypic manifestations are critical. Such efforts could help researchers mitigate etiological heterogeneity in their samples, leading to improvements in recurrence estimation and enhancing gene identification approaches.

Another challenge for future studies in this area will be documenting brain shape in nonsyndromic clefting across different age groups. In a recent volumetric study, Nopoulos et al. (2007a) found that both affected boys and girls (age 7–17) had significant reductions in total brain, cerebral, and cerebellar volume compared with matched controls, even after adjusting for body size. In terms of individual cerebral regions, the child cleft sample had reduced frontal lobe and increased occipital lobe volumes, with no change in the parietal and temporal lobes. This pattern of altered regional brain morphology is strikingly different from that observed in the present study, suggesting that the trajectory of brain development may be altered across the lifespan. A longitudinal follow-up study on this adolescent sample is currently underway, providing an

opportunity to document ontogenetic changes in brain shape in relation to orofacial clefting.

Acknowledgements

Thank you to the many individuals who agreed to participate in this study. This research was supported by a Basil O'Connor Award from the March of Dimes #5-FY98–0541 and the following grants from the National Institutes of Health: R01-MH-040856; R01-MH-031593; T32-MH-019113.

References

Abzhanov A, Cordero DR, Sen J, Tabin CJ, Helms JA (2007) Cross-regulatory interactions between Fgf8 and Shh in the avian frontonasal prominence. *Congenit Anom* **47**, 136–148.

Aduss H, Pruzansky S, Miller M (1974) Interorbital distance in cleft lip and palate. *Teratology* **4**, 171–182.

Andreasen NC, Cohen G, Harris G, et al. (1992) Image processing for the study of brain structure and function: problems and programs. *J Neuropsychiatry Clin Neurosci* **4**, 125–133.

Antshel KM, Conchelos J, Lanzetta G, Fremont W, Kates WR (2005) Behavior and corpus callosum morphology relationships in velocardiofacial syndrome (22q11.2 deletion syndrome). *Psychiatry Res* **138**, 235–245.

Bergsma D (1975) *Morphogenesis and Malformation of Face and Brain*. New York: Alan R. Liss, Inc.

Bertrand N, Dahmane N (2006) Sonic hedgehog signaling in forebrain development and its interactions with pathways that modify its effects. *Trends Cell Biol* **16**, 597–605.

Bodensteiner JB, Schaefer GB (1990) Wide cavum septum pellucidum: a marker of disturbed brain development. *Pediatr Neurol* **6**, 391–394.

Boes AD, Murko V, Wood JL, et al. (2007) Social function in boys with cleft lip and palate: relationship to ventral frontal cortex morphology. *Behav Brain Res* **181**, 224–231.

Boger-Megiddo I, Shaw DW, Friedman SD, et al. (2006) Corpus callosum morphometrics in young children with autism spectrum disorder. *J Autism Dev Disord* **36**, 733–739.

Bookstein FL, Sampson PD, Streissguth AP, Connor PD (2001) Geometric morphometrics of corpus callosum and subcortical structures in the fetal-alcohol-affected brain. *Teratology* **6**, 4–32.

Brennan DG, Cullinan WL (1974) Object identification and naming in cleft palate children. *Cleft Palate J* **11**, 188–195.

Broen PA, Devers MC, Doyle SS, Prouty JM, Moller KT (1998) Acquisition of linguistic and cognitive skills by children with cleft palate. *J Speech Lang Hear Res* **41**, 676–687.

Calzolari E, Pierini A, Astolfi G, Bianchi F, Neville AJ, Rivieri F (2007) Associated anomalies in multi-malformed infants with cleft lip and palate: An epidemiologic study of nearly 6 million births in 23 EUROCAT registries. *Am J Med Genet Part A* **143**, 528–537.

Campbell LE, Daly E, Toal F, et al. (2006) Brain and behaviour in children with 22q11.2 deletion syndrome: a volumetric and voxel-based morphometry MRI study. *Brain* **129**, 1218–1228.

Casanova MF, Sanders RD, Goldberg TE, et al. (1990) Morphometry of the corpus callosum in monozygotic twins discordant for schizophrenia: a magnetic resonance imaging study. *J Neurol Neurosurg Psychiatry* **53**, 416–421.

Cole TM (2003) *WinEDMA: Software for Euclidean Distance Matrix Analysis*. Kansas City: University of Missouri-Kansas City School of Medicine.

Creuzet S, Schuler B, Couly G, Le Douarin NM (2004) Reciprocal relationships between Fgf8 and neural crest cells in facial and forebrain development. *Proc Natl Acad Sci U S A* **101**, 4843–4847.

Diewert VM, Lozanoff S, Choy V (1993) Computer reconstructions of human embryonic craniofacial morphology showing changes in relations between the face and brain during primary palate formation. *J Craniofac Genet Dev Biol* **13**, 193–201.

Downhill JE, Buchsbaum MS, Wei T, et al. (2000) Shape and size of the corpus callosum in schizophrenia and schizotypal personality disorder. *Schizophr Res* **42**, 193–208.

Eliez S, Schmitt JE, White CD, Reiss AL (2000) Children and adolescents with velocardiofacial syndrome: a volumetric MRI study. *Am J Psychiatry* **157**, 409–415.

Estes RE, Morris HL (1970) Relationships among intelligence, speech proficiency, and hearing sensitivity in children with cleft palates. *Cleft Palate J* **7**, 763–773.

Fox D, Lynch J, Brookshire B (1978) Selected developmental factors of cleft palate children between two and thirty-three months of age. *Cleft Palate J* **15**, 239–245.

Francis-West PH, Robson L, Evans DJ (2003) Craniofacial development: the tissue and molecular interactions that control development of the head. *Adv Anat Embryol Cell Biol* **169**, 1–138.

Fraser FC, Rex A (1985) Excess of parental non-righthandedness in children with right-sided cleft lip: a preliminary report. *J Craniofac Genet Dev Biol* Suppl 1, 85–88.

Goldstein JM, Seidman LJ, Horton NJ, et al. (2001) Normal sexual dimorphism of the adult human brain assessed by in vivo magnetic resonance imaging. *Cereb Cortex* **11**, 490–497.

Goodall CR (1991) Procrustes methods in the statistical analysis of shapes. *J R Stat Soc B* **53**, 285–339.

Graham A (2003) The neural crest. *Curr Biol* **13**, R381–R384.

Halilagic A, Ribes V, Ghyselinck NB, Zile MH, Dollé P, Studer M (2007) Retinoids control anterior and dorsal properties in the developing forebrain. *Dev Biol* **303**, 362–375.

Hallgrímsson B, Dorval CJ, Zelditch ML, German RZ (2004) Craniofacial variability and morphological integration in mice susceptible to cleft lip and palate. *J Anat* **205**, 501–517.

Hinrichsen K (1985) The early development of morphology and patterns of the face in the human embryo. *Adv Anat Embryol Cell Biol* **98**, 1–79.

Hu D, Helms JA (1999) The role of sonic hedgehog in normal and abnormal craniofacial morphogenesis. *Development* **126**, 4873–4884.

Hu D, Marcucio RS, Helms JA (2003) A zone of frontonasal ectoderm regulates patterning and growth in the face. *Development* **130**, 1749–1758.

Jeffery SLA, Boorman JG (2000) Left or right hand dominance in children with cleft lip and palate. *Br J Plast Surg* **53**, 477–478.

Jeong J, Mao J, Tenzen T, Kottmann AH, McMahon AP (2004) Hedgehog signaling in the neural crest cells regulates the patterning and growth of facial primordia. *Genes Dev* **18**, 937–951.

Jiang R, Bush JO, Lidral AC (2006) Development of the upper lip: morphogenetic and molecular mechanisms. *Dev Dyn* **235**, 1152–1166.

Jones KL (2006) *Smith's Recognizable Patterns of Human Malformation*. Philadelphia: Elsevier Saunders.

Jugessur A, Murray JC (2005) Orofacial clefting: recent insights into a complex trait. *Curr Opin Genet Dev* **15**, 270–278.

Kates WR, Burnette CP, Jabs EW, et al. (2001) Regional cortical white matter reductions in velocardiofacial syndrome: a volumetric MRI analysis. *Biol Psychiatry* **49**, 677–684.

Kilian S, Brown WS, Hallam BJ, et al. (2008) Regional callosal morphology in autism and macrocephaly. *Dev Neuropsychol* **33**, 74–99.

Kjaer I (1995) Human prenatal craniofacial development related to brain development under normal and pathological conditions. *Acta Odontol Scand* **53**, 135–143.

Klingenberg CP (2008) *MorphoJ*. Manchester: University of Manchester.

Kommers MS, Sullivan MD (1979) Written language skills of children with cleft palate. *Cleft Palate J* **16**, 81–85.

Le Douarin NM, Kalcheim C (1999) *The Neural Crest*. Cambridge, UK: Cambridge University Press.

Lele S, Richtsmeier J (2001) *An Invariant Approach to the Statistical Analysis of Shapes*. Boca Raton: Chapman and Hall/CRC.

Lidral AC, Moreno LM (2005) Progress toward discerning the genetics of cleft lip. *Curr Opin Pediatr* **17**, 731–739.

MacDonald ME, Abbott UK, Richman JM (2004) Upper beak truncation in chicken embryos with the cleft primary palate mutation is due to an epithelial defect in the frontonasal mass. *Dev Dyn* **230**, 335–349.

Machado AM, Simon TJ, Nguyen V, McDonald-McGinn DM, Zackai EH, Gee JC (2007) Corpus callosum morphology and ventricular size in chromosome 22q11.2 deletion syndrome. *Brain Res* **1131**, 197–210.

Magnotta VA, Heckel D, Andreasen NC, et al. (1999a) Measurement of brain structures with artificial neural networks: two- and three-dimensional applications. *Radiology* **211**, 781–790.

Magnotta VA, Andreasen NC, Schultz SK, et al. (1999b) Quantitative in vivo measurement of gyrification in the human brain: changes associated with aging. *Cereb Cortex* **9**, 151–160.

Magnotta VA, Harris G, Andreasen NC, O'Leary DS, Yuh WT, Heckel D (2002) Structural MR image processing using the BRAINS2 toolbox. *Comput Med Imaging Graph* **26**, 251–264.

Marazita ML (2007) Subclinical features in non-syndromic cleft lip with or without cleft palate (CL/P): review of the evidence that subepithelial orbicularis oris muscle defects are part of an expanded phenotype for CL/P. *Orthod Craniofacial Res* **10**, 82–87.

Marcucio RS, Cordero DR, Hu D, Helms JA (2005) Molecular interactions coordinating the development of the forebrain and face. *Dev Biol* **284**, 48–61.

Mueller AA, Sader R, Honigmann K, Zeilhofer HF, Schwenzer-Zimmerer K (2007) Central nervous malformations in presence of clefts reflect developmental interplay. *Int J Oral Maxillofac Surg* **36**, 289–295.

Narr KL, Thompson PM, Sharma T, Moussai J, Cannestra AF, Toga AW (2000) Mapping morphology of the corpus callosum in schizophrenia. *Cereb Cortex* **10**, 40–49.

Neiman GS, Savage HE (1997) Development of infants and toddlers with clefts from birth to three years of age. *Cleft Palate Craniofac J* **34**, 218–225.

Nopoulos P, Berg S, VanDemark D, Richman L, Canady J, Andreasen NC (2001) Increased incidence of a midline brain anomaly in patients with nonsyndromic clefts of the lip and/or palate. *J Neuroimaging* **11**, 418–424.

Nopoulos P, Berg S, Canady J, Richman L, Van Demark D, Andreasen NC (2002) Structural brain abnormalities in adult males with clefts of the lip and/or palate. *Genet Med* **4**, 1–9.

Nopoulos P, Choe I, Berg S, Van Demark D, Canady J, Richman L (2005) Ventral frontal cortex morphology in adult males with isolated orofacial clefts: relationship to abnormalities in social function. *Cleft Palate Craniofac J* **42**, 138–144.

Nopoulos P, Flaum M, O'Leary D, Andreasen NC (2000) Sexual dimorphism in the human brain: evaluation of tissue volume, tissue composition and surface anatomy using magnetic resonance imaging. *Psychiatry Res* **98**, 1–13.

Nopoulos P, Langbehn DR, Canady J, Magnotta V, Richman L (2007a) Abnormal brain structure in children with isolated clefts of the lip and palate. *Arch Pediatr Adolesc Med* **161**, 753–758.

Nopoulos P, Richman L, Andreasen NC, Murray JC, Schutte BC (2007b) Abnormal brain structure in adults with Van der Woude syndrome. *Clin Genet* **71**, 511–517.

O'Higgins P, Jones N (1998) Facial growth in Cercocebus torquantus: an application of three-dimensional geometric morphometric techniques to the study of morphological variation. *J Anat* **193**, 251–272.

Orioli IM, Vieira AR, Castilla EE, Ming JE, Muenke M (2002) Mutational analysis of the sonic hedgehog gene in 220 newborns with oral clefts in a South America (ECLAMC) population. *Am J Med Genet* **108**, 12–15.

Parsons TE, Kristensen E, Hornung L, et al. (2008) Phenotypic variability and craniofacial dysmorphology: increased shape variance in a mouse model for cleft lip. *J Anat* **212**, 135–143.

Rice R, Connor E, Rice DP (2006) Expression patterns of Hedgehog signaling pathway members during mouse palate development. *Gene Expr Patterns* **6**, 206–212.

Richards LJ, Plachez C, Ren T (2004) Mechanisms regulating the development of the corpus callosum and its agenesis in mouse and human. *Clin Genet* **66**, 276–289.

Richman LC (1980) Cognitive patterns and learning disabilities in cleft palate children with verbal deficits. *J Speech Hear Res* **23**, 447–456.

Richman LC, Elaison MJ (1993) Psychological characteristics associated with cleft palate. In *Cleft Palate: Interdisciplinary Issues and Treatment* (eds Moller KT, Starr CD), pp. 357–380. Austin, TX: Pro-Ed, Inc.

Richtsmeier JT, DeLeon VB, Lele SR (2002) The promise of geometric morphometrics. *Yearb Phys Anthropol* **46**, 63–91.

Rohlf F, Slice D (1990) Extensions of the Procrustes method for the optimal superimposition of landmarks. *Syst Zool* **39**, 40–59.

Rohlf FJ (1999) Shape statistics: Procrustes superimpositions and tangent spaces. *J Class* **16**, 197–223.

Rohlf FJ (2000) Statistical power comparisons among alternative morphometric methods. *Am J Phys Anthropol* **111**, 463–478.

Sak RJ, Ruben RJ (1982) Effects of recurrent middle ear effusion in preschool years on language and learning. *J Dev Behav Pediatr* **3**, 7–11.

Sarwar M (1989) The septum pellucidum: normal and abnormal. *Am J Neuroradiol* **10**, 989–1005.

Sasaki Y, O'Kane S, Dixon J, Dixon MJ, Ferguson MW (2007) Temporal and spatial expression of Pax9 and Sonic hedgehog during development of normal mouse palates and cleft palates in TGF-beta3 null embryos. *Arch Oral Biol* **52**, 260–267.

Schneider RA, Hu D, Rubenstein JL, Maden M, Helms JA (2001) Local retinoid signaling coordinates forebrain and facial morphogenesis by maintaining FGF8 and SHH. *Development* **128**, 2755–2767.

Senders CW, Peterson EC, Hendrickx AG, Cukierski MA (2003) Development of the upper lip. *Arch Facial Plast Surg* **5**, 16–25.

Shashi V, Muddasani S, Santos CC, et al. (2004) Abnormalities of the corpus callosum in nonpsychotic children with chromosome 22q11 deletion syndrome. *Neuroimage* **21**, 1399–1406.

Sheets HD (2004) *Simple3D: Integrated Morphometrics Package (IMP) Software Series*. Buffalo: Canisius College.

Shriver AS, Canady J, Richman L, Andreasen NC, Nopoulos P (2006) Structure and function of the superior temporal plane in adult males with cleft lip and palate: pathologic enlargement with no relationship to childhood hearing deficits. *J Child Psychol Psychiat* **47**, 994–1002.

Simon TJ, Ding L, Bish JP, McDonald-McGinn DM, Zackai EH, Gee J (2005) Volumetric, connective, and morphologic changes in the brains of children with chromosome 22q11.2 deletion syndrome: an integrative study. *Neuroimage* **25**, 169–180.

Sowell ER, Peterson BS, Kan E, et al. (2007) Sex differences in cortical thickness mapped in 176 healthy individuals between 7 and 87 years of age. *Cereb Cortex* **17**, 1550–1560.

Sperber GH (2001) *Craniofacial Development*. Hamilton, ON: BC Decker Inc.

Stanier P, Moore GE (2004) Genetics of cleft lip and palate: syndromic genes contribute to the incidence of non-syndromic clefts. *Hum Mol Genet* **13**, R73–R81.

Sulik KK, Johnston MC (1982) Embryonic origin of holoprosencephaly: interrelationship of the developing brain and face. *Scan Electron Microsc* **1**, 309–322.

Thomason HA, Dixon MJ, Dixon J (2008) Facial clefting in Tp63 deficient mice results from altered Bmp4, Fgf8 and Shh signaling. *Dev Biol* **321**, 273–282.

Tomaiuolo F, Di Paola M, Caravale B, Vicari S, Petrides M, Caltagirone C (2002) Morphology and morphometry of the corpus callosum in Williams syndrome: a T1-weighted MRI study. *Neuroreport* **13**, 2281–2284.

Vermeij-Keers C, Mazzola RF, Van der Meulen JCH, Strickler M (1983) Cerebro-craniofacial and craniofacial malformations: and embryological analysis. *Cleft Palate J* **20**, 128–145.

Weinberg SM, Maher BS, Marazita ML (2006a) Parental craniofacial morphology in cleft lip with or without cleft palate as determined by cephalometry: a meta-analysis. *Orthod Craniofacial Res* **9**, 18–30.

Weinberg SM, Neiswanger K, Martin RA, et al. (2006b) The Pittsburgh Oral-Facial Cleft Study: expanding the cleft phenotype. Background and justification. *Cleft Palate Craniofac J* **43**, 7–20.

Weinberg SM, Neiswanger K, Richtsmeier JT, et al. (2008) Three-dimensional morphometric analysis of craniofacial shape in the unaffected relatives of individuals with nonsyndromic orofacial clefts: a possible marker for genetic susceptibility. *Am J Med Genet Part A* **146**, 409–420.

Wentzlaff KA, Cooper ME, Yang P, et al. (1997) Association between non-right-handedness and cleft lip with or without cleft palate in a Chinese population. *J Craniofac Genet Dev Biol* **17**, 141–147.

Yorita GJ, Melnick M (1988) Cleft lip and handedness: a study of laterality. *Am J Med Genet* **31**, 273–280.

Young NM, Wat S, Diewert VM, Browder LW, Hallgrímsson B (2007) Comparative morphometrics of embryonic facial morphogenesis: implications for cleft-lip etiology. *Anat Rec* **290**, 123–139.

Zelditch ML, Swiderski DL, Sheets HD, Fink WL (2004) *Geometric Morphometrics for Biologists: A Primer*. Amsterdam: Elsevier Academic Press.